ISBN: 978-3-95450-249-3 ISSN: 2673-5350 doi: 10.18429/JACoW-IBIC2024-FRAT1

SECONDARY, THERMIONIC AND DELTA ELECTRON EMISSION FROM THIN TARGETS

M. Sapinski*
Paul Scherrer Institut, Villigen, Switzerland

Abstract

Thin objects in the form of wires, foils, or strips are often used as targets in various instruments that measure beam parameters, or for other purposes. They usually cause only small beam perturbations and suffer from relatively low temperature increases. The beam induces the emission of secondary electrons, which are typically the source of the measured signal. In high-brightness beams, the targets can reach high temperatures, leading to thermionic current emission. In addition, a certain number of delta electrons are emitted, which affects the emitted current as well as beam heating. These three types of electrons have different properties and influence the measured signal and the temperature evolution of the target. This paper discusses how the signal is generated by the escaping electrons, how the bunch field affects this signal, and how the target temperature depends on electron emission.

INTRODUCTION

Thin targets, in the form of micrometer-sized wires, strips, or foils, are widely used in particle accelerators, particularly in beam instrumentation. Their small thickness reduces the disturbance to the beam and damage to the targets themselves. Electron emission from these targets is often used as a signal to probe the beam distribution. There are multiple mechanisms of electron emission from the body exposed to radiation. The properties of these various electron emission processes are important for the correct interpretation of measurements obtained using beam instruments.

In this study, we discuss three types of electron emissions that are important for proton beam profile measurements using wire scanners and SEM-grids. They contribute to the electric current flowing to the wire, which is the signal used to measure beam parameters. They interact with the bunch fields and affect the thermal behavior of the targets. The three types of electron emission are delta, low-energy secondary, and thermionic. Other types of emissions, such as photoemission or emission of Auger electrons, are not relevant for this discussion.

Motivation

This study is particularly important for beam instruments that employ thin targets and measure the current generated by the beam interacting with these targets. Typically, these devices are SEM-grids or wire scanners that rely on the readout of electric current, which is used for low-energy beams that do not produce enough of a particle shower to be efficiently measured outside of the vacuum chamber. The phenomena discussed here are especially relevant for high-brightness beams, where the power deposited on the target is so high that it reaches temperatures at which thermionic emission becomes significant and affects the measured signal.

That being said, some of the results or discussions presented here are also partly applicable to other beam conditions and types of beams.

Study Cases

The mechanisms of secondary and delta electron generation have been studied for four specific cases of proton beams at the following energies:

- 72 MeV, as in case of beam extracted from PSI's Injector 2 cyclotron.
- 590 MeV, as in case of beam extracted from PSI's Main Ring cyclotron [1].
- 3 GeV, as in case of J-PARC Main Ring synchrotron at injection [2]; while this scanner uses 7 μm carbon fiber, for ease of comparison, calculations are done for 33 μm fibers.
- 450 GeV, as in case of CERN SPS flat top [3].

Due to the high brightness of the beams under consideration, the primary target material studied is carbon fiber (CF) [1], which is considered the gold standard for handling extremely challenging beam conditions (high brightness). However, additional calculations have been performed for molybdenum, which offers a good compromise between material density and high melting temperature, as well as tungsten, which has the highest melting temperature of all metals.

THIN TARGETS

The targets are considered thin when their thickness ranges from a few micrometers to approximately 100 μm. Typically, the targets take the shape of wires with a round cross-section or foils. In this study, we focus on thin wires with a diameter of 33 μm, which is smaller than average human hair (75 μm). Even thinner targets exist, such as foils with sub-micrometer thickness (down to 25 nm). They are used in accelerators for stripping electrons out of H^- ions in charge-exchange injection or extraction processes.

In case of such ultra-thin targets, the number of particle interactions with material electrons is so low (a few), that the energy straggling function exhibits a unique shape with multiple peaks at low energy and a long high-energy tail [4]. For micrometer-size targets a Landau distribution of straggling is an accurate approximation.

* mariusz.sapinski@psi.ch

[1] The density of the carbon fibre used in the simulations is 2 g/cm^3, however the values found in the literature vary between 1.7 and 2.1 g/cm^3.

Content from this work may be used under the terms of the CC BY 4.0 licence (© 2024). Any distribution of this work must maintain attribution to the author(s), title of the work, publisher, and DOI.

ISBN: 978-3-95450-249-3 ISSN: 2673-5350 doi: 10.18429/JACoW-IBIC2024-FRAT1

Content from this work may be used under the terms of the CC BY 4.0 licence (© 2024). Any distribution of this work must maintain attribution to the author(s), title of the work, publisher, and DOI.

Another characteristics of thin targets is that the energy deposited by the impacting particles is strongly reduced by electrons escaping the target and therefore removing part of the ionisation energy.

DELTA ELECTRONS

When a charged particle collides with an electron in a medium, the energy transfer can be large enough to produce a high-energy electron. These electrons often have sufficient energy to cause further ionization in the material, potentially even ejecting tertiary electrons. They are known as "delta-rays", the term which was first used by J.J. Thomson, who discovered the electron.

The maximum energy transfer to the electron, in case of binary collision with a zero impact parameter, is calculated from the principles of conservation of momentum and kinetic energy:

$$T_{\max} = \frac{2m_e c^2 \beta^2 \gamma^2}{1 + \frac{2\gamma m_e}{M} + (\frac{m_e}{M})^2} \qquad (1)$$

where and are relativistic parameters of the incident particle and M is its mass. For small impact parameters, the electron is emitted in the direction of the projectile. However, such cases are rare and most electrons are ejected from the target at large angles with respect to the beam direction, carrying energies lower than $T_{\max}$. Additionally, electrons scatter within the material, complicating the estimation of their properties. Therefore, it is recommended to use a particle transport code to determine their spectrum and angular distribution. The results presented in this study were obtained using Geant4 version 11.2 [5] with the G4EMStandardPhysics_option4 physics list.

Table 1 shows results obtained from Eq. (1) and the Geant4 simulation. For example, in the case of 590 MeV protons, the energy of produced electrons can reach up to 1.69 MeV, but the average energy is only 92 keV. The range of 92 keV electrons in graphite is approximately 100 µm, allowing them to escape from the target. However, only about 2 out of 100 protons crossing the target generate delta electrons.

The spectrum of electrons for various proton beam energies obtained with Geant4 is shown in Fig. 1. It follows E_δ^{-2} relation with corrections for energies near $T_{\max}$ [6, 7]. For very low energies, below about 100 eV, the spectrum shows structures related to atomic shells. However, this low energy part of the spectrum is strongly suppressed during the transport in the material and is negligible in comparison to low energy secondary electrons.

Table 1: Maximum and Average Energy of Delta Electrons For 33 µm Carbon Fibre

proton energy	$T_{\max}$	**emm.prob**	E_{avg}
72 MeV	160 keV	7.34 %	3 keV
590 MeV	1.69 MeV	1.93 %	92 keV
3 GeV	17 MeV	1.34 %	150 keV
450 GeV	155 GeV	1.29 %	297 keV

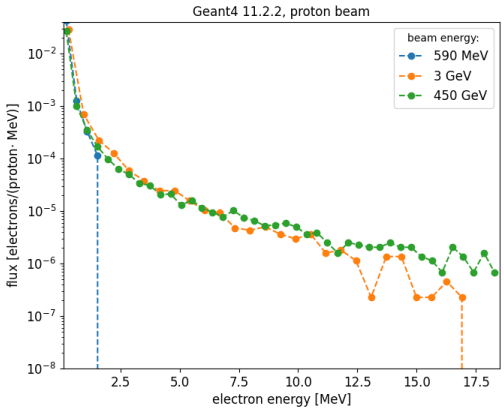

Figure 1: Spectra of delta electrons for various beam energies. The $T_{\max}$ is visible at 1.7 MeV for 590 MeV and 17 MeV for 3 GeV beams.

The probability of electron emission increases with the density of the material. For instance, for 590 MeV beam, a molybdenum wire generates 70 % more electrons while tungsten wire generates almost twice more. At high energies, this increase becomes even more pronounced.

The emission probability also depends on the thickness of the target. The number of electron increases rapidly with wire diameter but, as thicker targets also stop more electrons, the increase slows down. This kind of "saturation" effect can be observed in Fig. 2. It is especially strong for dense targets.

However, when the target thickness reach the radiation length of the material, which for the tungsten is only 3.5 mm, a sharp increase in electron yield is observed for high energy beams. This effect is due to the onset of an electromagnetic shower, not the ionization process. Therefore, these electrons are no longer delta electrons, they originate from pair production process.

High-Energy Electron From Other Processes

Plotting the dependence of electron energy (E_δ) and emission angle (Θ) for various Geant4 particle production processes, as shown in Fig. 3, provides an interesting insight. In this figure, prepared for 450 GeV beam, the blue points represent the real delta electrons, which originate from beam protons (with negligible contribution from secondary hadrons) interacting with material electrons (hIoni process). Their dependence of angle versus energy follows curve, which is characteristic for binary encounter: $E_\delta = T_{\max} \cos^2 \Theta$. This reflects the fact that when the impact parameter is close to zero, the energy transfer is large and the recoil angle is small. Therefore, only the most energetic delta electrons are emitted in the beam direction.

The large, dominant "band" of low energy electrons (1–100 keV in Fig. 3) emitted in all directions can be interpreted as delta electrons that undergo multiple scattering

ISBN: 978-3-95450-249-3 ISSN: 2673-5350 doi: 10.18429/JACoW-IBIC2024-FRAT1

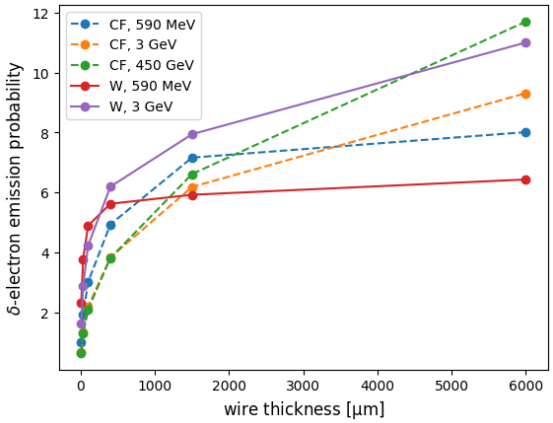

Figure 2: Delta electron emission probability per impacting proton as a function of target thickness for carbon and tungsten wires.

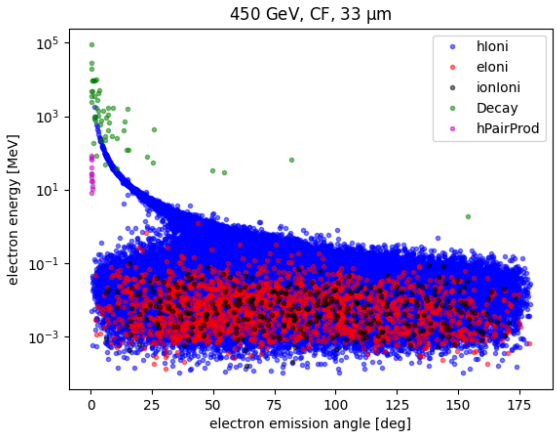

Figure 3: Plot of emission angle versus electron energy for all electrons leaving the target registered in Geant4 simulation.

events, tertiary electrons produced by delta electrons (eIoni process) and electrons produced by atomic recoils (ionIoni process). The actual angular distribution is broad, with a peak at about 70°, as shown in Fig. 4.

Apart of ionisation, electrons are produced in other two processes: pair creation and a decay of other particles. As stated in previous section, pair production marks the onset of electromagnetic cascade, which is not strongly developed in thin carbon fiber. The decay of other particles produces a very small number of electrons, however these electrons have high energies and are produced in forward direction. Averaging energy of these electrons over all protons traversing the target gives a remarkable value of 23.6 keV. These electrons do not contribute to the correction of the energy deposit in the target, which is discussed in the next section.

Correction to Energy Deposit

The Bethe-Bloch formula describes the energy loss of a charged particles to the electrons in the medium. This formula gives an estimation to energy deposit, if all the

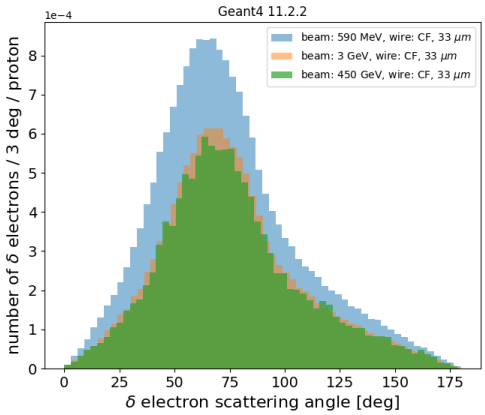

Figure 4: Angular distribution of electrons emitted from 33 μm carbon fiber for various impacting beam energies.

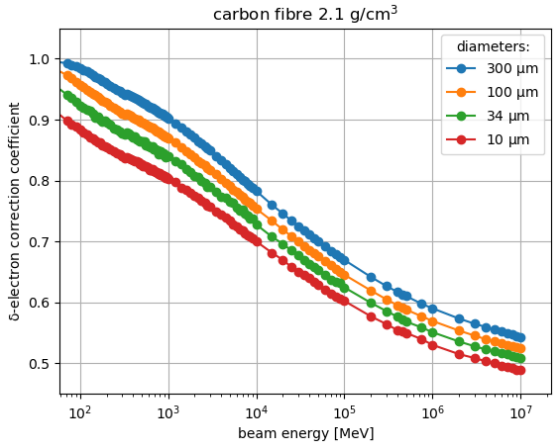

Figure 5: Delta-electron correction coefficient (see text).

energy loss is confined within the target. However, the high-energy delta electrons carry away a significant amount of this energy. This fact has been investigated already in [8], where an simplified calculation was used to estimate that "up to 70 % of the incident proton energy loss can be accounted for in this way".

The amount of energy carried away by the electrons depends on the beam energy, the target thickness and the material. The ratio of real beam energy deposit in the target per proton (E_{dep}) to the expected value from Bethe-Bloch formula defines the "δ-electron correction coefficient". Geant4 simulations have been performed to investigate the value of this coefficient for various wire thicknesses and various beam energies. Figure 5 shows the results of these simulations. Indeed, at high protons energies up to 50 % of the ionisation energy leaves the target, while at low energies this effect is very small.

LOW ENERGY SECONDARY ELECTRONS

When the collisions of the projectile with material electrons become peripheral, more electrons are involved. At

Content from this work may be used under the terms of the CC BY 4.0 licence (© 2024). Any distribution of this work must maintain attribution to the author(s), title of the work, publisher, and DOI.

ISBN: 978-3-95450-249-3 ISSN: 2673-5350 doi: 10.18429/JACoW-IBIC2024-FRAT1

Content from this work may be used under the terms of the CC BY 4.0 licence (© 2024). Any distribution of this work must maintain attribution to the author(s), title of the work, publisher, and DOI.

large impact parameters this process, this process is more accurately described as an interaction with a plasma of electrons rather than binary collisions. The number of excited electrons is much larger than in case of binary collisions, but their energy is very low, below 100 eV. Therefore, only electrons created close to the surface of the target have a chance to escape. The probability of their creation is described by the modified Sternglass model [9].

It should be stressed that logically, all electrons emitted in proton interaction with material are "secondary" (protons are primary particles). However, due to historical reasons, the name "secondary electrons" is usually reserved only for the low-energy electrons produced at the surface and described by the Sternglass model. Here, we will use expression "low energy secondary electrons" to refer to these electrons.

Geant4 tracks delta electrons down to energies of 100 eV, and the complexity of the physics of very low energies is not within its scope of applications. Here, it is assumed that the Sternglass model fills the gap for electron energies between 0 and 100 eV. However, the choice of the borderline energy is somewhat arbitrary and may lead to errors in calculated yields. It is believed that these errors are small.

Sternglass Model

In the Sternglass model, low energy secondary electron creation is a three-step process: ionisation, transport and escape from the solid through the surface barrier. The number of ionizations is proportional to the projectile energy loss, i.e. dE/dx. The diffusion is driven by inelastic scatterings, in which electrons loose their energy. The typical distance between inelastic collisions is expressed by Eq. (2), and ranges from 0.93 nm for tungsten to 1.4 nm for carbon.

$$L_S = \left(3.68 \cdot 10^{-17} N_v Z^{1/3}\right)^{-1} \tag{2}$$

Finally, the electrons must overcome the surface barrier, losing a part of their energy. The total number of secondary electrons per proton or ion crossing the surface is expressed by Eq. (3). One can see that the SEY depends on the particle energy similarly to Bethe-Bloch.

$$SEY = 0.01 L_S \left.\frac{dE}{dx}\right|_{el} \left[1 + \frac{1}{1 + 5.4 \cdot 10^{-6} E/A_p}\right] \tag{3}$$

The SEY for different beam energies and materials is calculated in Table 2.

Table 2: Secondary Emission Yield (SEY) Assuming That the Protons Cross Two Surfaces (Go Through the Target)

proton energy	Carbon	Mo	Tungsten
72 MeV	4.06 %	14.87 %	21.69 %
590 MeV	1.14 %	4.19 %	6.11 %
3 GeV	0.93 %	3.42 %	4.99 %
450 GeV	1.66 %	6.06 %	8.84 %

The real yield depends not only on the material but also on the quality of the surface and surface treatment. For instance, long exposure to radiation often decreases SEY. This type of surface conditioning is sometimes called "scrubbing" [10].

Spectrum

In his original article, Sternglass observes that the spectrum of secondary electrons has the same form for all metals and drops sharply for energies above 10–15 eV. However, measurements (see e.g. [11]), often show spectral differences between various materials or even surfaces. These differences do not affect the second observation that the peak of the spectrum is below 5 eV and most secondary electrons have energies below 20 eV. This means that, in contrast to delta electrons, low energy secondary electrons carry away a negligible amount of thermal energy from the target.

Delta and Secondary Electron Yields

Comparing the delta electron emission probability from Table 1 with SEY values from Table 2 one can see that these values are not very different. Table 3 summarizes the contribution of low energy secondary electrons to the total signal registered from various target materials.

As seen from this table, low energy secondary electrons do not dominate the total signal. Especially for low density targets and low beam energy, their contribution is less than half. This is an important fact for targets operated with bias voltage, as a method to circumvent the thermionic emission.

Experimental Evidence

In order to verify whether the electrons emitted from the wire have low or high energies, it is useful to observe the change of the signal amplitude as a function of the bias voltage. A positive bias voltage of a few volts should attract low energy secondary electrons back to the wire, effectively reducing the observed signal. Such an experiment has been performed using Keithley 4200 source meter and for wire position fixed in one location inside the beam. The results, shown in Fig. 6, indeed show a strong reduction of the signal with the bias voltage, although the decrease appears to require stronger bias potentials than expected from the properties of secondary electron spectra.

THERMIONIC ELECTRONS

Emission of electric current from hot metals in vacuum was first observed in 1853 by the French physicist Edmond

Table 3: Secondary Emission Yield (SEY) Contribution to the Total Electric Current Emitted From 33 μm Wires

proton energy	Carbon	Mo	Tungsten
72 MeV	36 %	62 %	71 %
590 MeV	37 %	56 %	62 %
3 GeV	41 %	57 %	64 %
450 GeV	57 %	72 %	76 %

ISBN: 978-3-95450-249-3 ISSN: 2673-5350 doi: 10.18429/JACoW-IBIC2024-FRAT1

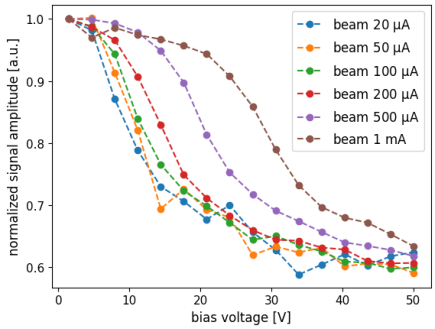

Figure 6: Measurements of the wire signal with changing bias voltage and for various beam intensities. Courtesy of J. Touguet.

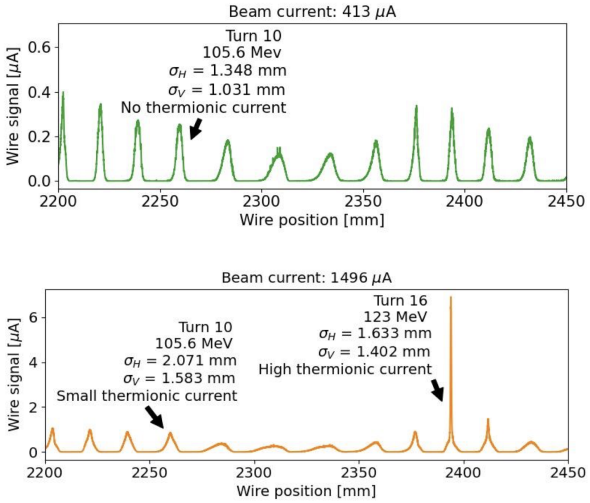

Figure 7: Example of thermionic emission observed in PSI Main Ring Long Radial Probe [13]

.

Becquerel. In 1911, Owen Richardson published a theory of thermionic emission [12], in which the thermionic current density is described by Eq. (4), where A_G is Richardson-Dushmann constant and Φ is material work function.

$$J_{th} = A_G T^2 e^{\frac{-\Phi}{k_B T}} \tag{4}$$

An example of thermionic emission can be seen in Fig. 7, which shows a partial profile of the orbits measured in the PSI Main Ring cyclotron. Two measurements are shown, at beam current of 417 µA and 1.5 mA. Arrows point at orbits in which a combination of beam energy and transverse beam dimensions lead to excessive heating and thermionic emission. In the case of the orbit at radius of about 2350 mm the amplitude of the thermionic current is several times higher than the normal signal.

Spectrum

The shape of the thermionic electron spectrum is expressed by Eq. (5).

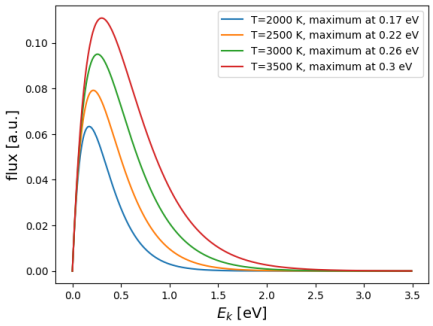

Figure 8: Examples of thermionic electron spectra for various temperatures of carbon (Φ = 4.8 eV) target.

$$N(E) \propto E e^{\frac{\Phi - E}{k_B T}} \tag{5}$$

The resulting curves are shown, for various temperatures, in Fig. 8. Even in the case of extremely hot wires, the peak of the kinetic energy of emitted electrons is below 1 eV, so they have energies even lower than secondary emission electrons.

Remnant Thermionic Current

Thermionic current distorts the measurement of the beam profile. The usual way of dealing with this distortion is the application of a positive bias voltage, which acts on thermionic electrons but allows the secondary electrons to be released. However, as noted already in [14]: "It is remarkable that the positive bias of the wire catches thermionically emitted electrons much better than secondary electrons from the wire, although both are mostly slow. This is probably due to the fact that all the secondary electrons created by the bunch are born in the bunch potential which pulls them away, while most of time (i.e. between the bunches) the bias potential retards the termionically emitted electrons."

As shown in Table 3, the effect of the bias potential not affecting the detector signal can be partly explained by the significant contribution of high-energy delta electrons to this signal. However delta electrons cannot explain this effect completely. Figure 6 clearly shows the impact of the beam intensity and, therefore, the bunch potential. Additionally, it has been reported in [15] that, despite the increase in the bias voltage, some thermionic current remains visible in the signal, as shown in Fig. 9. This suggests that the bunch field is being able to carry away low energy electrons.

Thermionic Cooling Effect

The removal of the highest-energy thermal electrons from the material is analogous to the phenomena of boiling liquid and has similarly strong cooling effect. This effect, discussed in [16], is the dominant cooling mechanism for carbon at temperatures above 3200 K. Below that temperature, radiative cooling, which is proportional to fourth power of temperature, dominates. A simplified formula describing the wire temperature evolution is shown in Eq. (6), where d is the wire diameter, ρ is the density and c_p is the specific heat of the wire material.

Content from this work may be used under the terms of the CC BY 4.0 licence (© 2024). Any distribution of this work must maintain attribution to the author(s), title of the work, publisher, and DOI.

ISBN: 978-3-95450-249-3 ISSN: 2673-5350 doi: 10.18429/JACoW-IBIC2024-FRAT1

Content from this work may be used under the terms of the CC BY 4.0 licence (© 2024). Any distribution of this work must maintain attribution to the author(s), title of the work, publisher, and DOI.

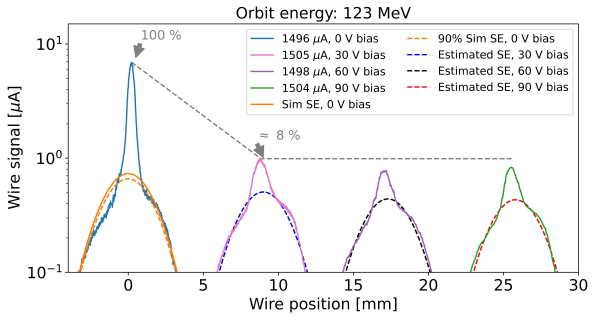

Figure 9: Illustration of remnant thermionic emission, Figure from [15].

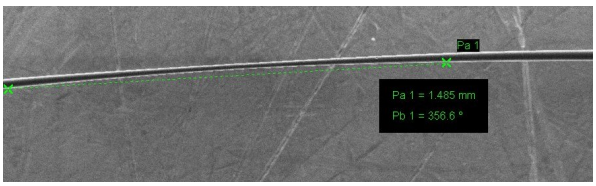

Figure 10: Electron microscope image of partly-sublimated wire from LHC scanner (from [16]).

$$\frac{\delta T}{\delta t} = \frac{N_{\text{wire}}(t)}{c_p(T)} E_{\text{dep}} - \frac{4\sigma_{SB}\epsilon}{d\rho c_p}(T^4 - T_0^4) - (\Phi + \frac{2k_B T}{q_e})\frac{4J_{th}(T)}{d\rho c_p} \quad (6)$$

However, at temperature of 3200 K, the carbon vapour pressure is high enough to observe a significant sublimation rate. Figure 10 shows partial sublimation of the wire repeatedly exposed to the high-brightness LHC beam. It is worth noticing that sublimation acts as a negative feedback mechanism: a thinner wire has a larger surface-to-volume ratio, so the cooling power, which is proportional to the surface area of the wire, decreases much slower than the heating power, which is proportional to the volume. In this case, gentle sublimation leads to thinning of the wire, which leads to a decrease in the wire temperature during subsequent scans and a decrease in the sublimation rate. This wire never broke in the machine and was successfully used to measure the beams size.

Space-Charge Limit

The thermionic emission current can easily be much stronger than low energy secondary or delta electron currents. Because of the small emitting surface, the question of current density and the impact of the electron space charge on the signal should be investigated.

Figure 11, originally from [13], shows a beam profile measured by RRL featuring a large thermionic emission contribution. Attempts to simulate the current evolution using PyTT [17] code, with various parametrisations of work function as a function of temperature and varying other parameters, were not successful.

The question arises whether the electron current emitted from the wire is strong enough to affect the electric field around the wire. The current density corresponding to

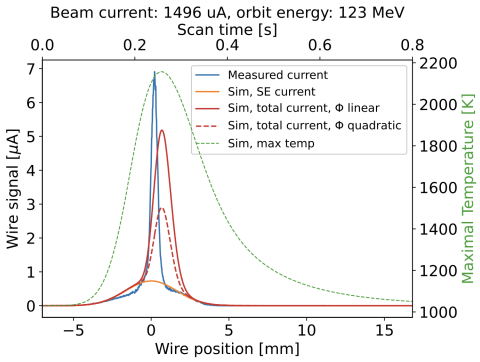

Figure 11: Measurement of the beam profile of high-brightness orbit using RRL. Courtesy of M. Boucard [15].

the signal shown in Fig. 11 is between 50 and 100 A/m^2 at the wire surface. On the other hand, the Child-Langmuir law [18] describing the space-charge limit to the current emitted from a flat cathode gives about 300 A/m^2. Given the uncertainties, those numbers are not very different. Therefore, a study of the thermionic electron cloud space charge effect on the wire signal is ongoing.

INTERACTION WITH BUNCH FIELD

The interaction of low energy electrons from residual gas ionisation with the beam field has been studied in [19–21]. It shows that high-brightness relativistic bunches are able to "trap" electrons from residual gas ionization inside the bunch field for the duration of the bunch passage and give them a significant momentum "kick".

The energies of low energy secondary and thermionic electrons are below 100 eV, similarly to electrons from gas ionization. The main difference is the presence of the field from the wire, whether biased or not. Additionally, the studies mentioned before regarded ultra-relativistic beams where longitudinal electric field could be neglected. This is not a case for PSI beams with energies between 72 and 590 MeV.

The study of this effect is being carried out using the Virtual-IPM [22] and CST studio [23] programs. Preliminary results show that indeed some of the electrons can get additional kick from the beam field and drift away from the wire despite of the bias voltage. A separate publication of this study is planned.

SUMMARY AND CONCLUSIONS

This study outlines some interesting facts concerning the beam diagnostic devices that employ secondary emission electrons to measure high-brightness beams, namely:

- Delta electrons with energies in keV-range give a significant contribution to the signal, especially for low-density targets like carbon fibre.
- Experiments show that the beam field affects the measured electron current.
- Preliminary results show that the beam field could be at least partly responsible for the part of the thermionic

ISBN: 978-3-95450-249-3 ISSN: 2673-5350 doi: 10.18429/JACoW-IBIC2024-FRAT1

Table 4: Properties of Electrons Emitted in Various Processes

electrons	delta	secondary	thermionic
energy	> 100 eV	< 100 eV	< 10 eV
max currrent	1 µA	1 µA	10 µA
prop to beam	yes	yes	no
affected by bias	no	yes	yes
cooling effect	yes	no	yes

current that is not removed from the signal by the bias voltage.

- Delta-electrons carry away a large portion of the ionization energy that would otherwise be left in the target by the impacting protons.
- Thermionic current is a very efficient cooling mechanism; unfortunately its highest efficiency overlaps with temperatures at which the carbon sublimation rate is substantial.
- Large thermionic current maybe limited by the space charge of thermionic electrons.

The properties of the three considered electron types are outlined in Table 4.

This publication does not exhaust the subject. Many of presented ideas need simulations or detailed calculations to be confirmed or even ruled out. Ultimately, the planned study should propose a solution to the issue of the remaining thermionic emission, which is actually a problem of some wire scanners working on high-brightness beams.

ACKNOWLEDGEMENTS

The author would like to express sincere gratitude to all those who contributed to this work through insightful discussions, dedicated efforts, and inspiring ideas. In particular, special thanks go to Rudolf Doelling, Jerome Touguet, Manon Boucard, Dominik Vilsmeier, Araceli Navarro, Hui Zhang, Richard Kan, Peter Forck, Jak Koopman, Plamen Boutachkov, and Kenichiro Satou. Their invaluable contributions, ranging from technical expertise and coding efforts to intellectual input, were instrumental in the successful completion of this research. The author also extends appreciation to the many others whose support and collaboration were vital to this work.

REFERENCES

[1] M. Sapinski, R. Doelling, and M. Rohrer, "Commissioning of the Renewed Long Radial Probe in PSI Ring Cyclotron", in *Proc. IBIC'22*, Kraków, Poland, Sep. 2022, pp. 76–79. doi:10.18429/JACoW-IBIC2022-MOP19

[2] S. Igarashi, D. A. Arakawa, Y. Hashimoto, M. Tejima, T. Toyama, and K. Hanamura, "Flying Wire Beam Profile Monitors at the J-PARC MR", in *Proc. IBIC'12*, Tsukuba, Japan, Oct. 2012, paper TUPB78, pp. 527–530.

[3] S. Di Carlo *et al.*, "Commissioning of the LHC Injectors Upgrade fast wire scanners and first experimental results", *Nucl. Instrum. Meth. A*, vol. 1053, p. 168328, 2023. doi:10.1016/j.nima.2023.168328

[4] H. Bichsel and R. Saxon, "Comparison of calculational methods for straggling in thin absorbers", *Phys. Rev. A*, vol. 11, pp. 1286–1296, 1975. doi:10.1103/PhysRevA.11.1286

[5] J. Allison *et al.*, "Recent developments in Geant4", *Nucl. Instr. Meth. A*, vol. 835, pp. 86–225, 2016. doi:10.1016/j.nima.2016.06.125

[6] M. E. Rudd, Y.-K. Kim, D. H. Madison, and T. J. Gay, "Electron production in proton collisions with atoms and molecules: energy distributions", *Rev. Mod. Phys.*, vol. 64, pp. 441–490, 1992. doi:10.1103/RevModPhys.64.441

[7] A. Akkerman, M. Murat and J. Barak, "Delta-electron spectra, inelastic cross sections, and stopping powers of ions in silicon: Comparison between different models", *Nucl. Instr. Meth. B*, vol. 321, pp. 1–7, 2014. doi:10.1016/j.nimb.2013.12.002

[8] J. Bosser *et al.*, "The Micron Wire Scanner at SPS", CERN, Geneva, Switzerland, Rep. CERN-SPS-86-26, Dec. 1986.

[9] E. J. Sternglass, "Theory of Secondary Electron Emission by High-Speed Ions", *Phys. Rev.*, vol. 108, no. 1, 1957. doi:10.1103/PhysRev.108.1

[10] G. Rumolo, H. Bartosik, E. Belli, P. Dijkstal, G. Iadarola, K. Li, L. Mether, A. Romano, M. Schenk, and F. Zimmermann, "Electron Cloud Effects at the LHC and LHC Injectors", in *Proc. IPAC'17*, Copenhagen, Denmark, May 2017, pp. 30–36. doi:10.18429/JACoW-IPAC2017-MOZA1.

[11] D. Hasselkamp, S. Hippler, and A Scharmann, "Ion-induced secondary electron spectra from clean metal surfaces", *Nucl. Instrum. Meth. B*, vol. 18, pp. 561–565, 1986. doi:10.1016/s0168-583x(86)80088-x

[12] O. W. Richardson, *The Emission of Electricity from Hot Bodies*. London: Longmans Green and Company, 1916.

[13] M. Boucard, "Thin targets in extreme conditions: probing high-brightness hadron beams", MSc thesis, EPFL Lausanne, Switzerland, 2023.

[14] R. Dölling, "Bunch-shape measurements at PSI's High-Power Cyclotrons and Proton Beam Lines", in *Proc. Cyclotrons'13*, Vancouver, Canada, 2013, paper TU3PB01, pp. 257–261.

[15] M. Boucard and M. Sapinski, "Dealing with thermionic emission in wire scanners based on secondary electron emission", in *Proc. IPAC'23*, Venice, Italy, May 2023, pp. 4820–4823. doi:10.18429/JACoW-IPAC2023-THPL150

[16] M. Sapinski, "Beam Interaction with Thin Materials: Heat Deposition, Cooling Phenomena and Damage Limits", in *Proc. BIW'12*, Newport News, VA, USA, Apr. 2012, pp. 245–249.

[17] https://github.com/ClaudePP/PyTT

[18] I. Langmuir, *The Effect of Space Charge and Residual Gases on Thermionic Currents in High Vacuum*, *Phys. Rev.*, vol. 2, pp. 450–486, 1913. doi:10.1103/PhysRev.2.450

[19] D.M. Vilsmeier, M. Sapinski, R. Singh, and J.W. Storey, "Reconstructing Space-Charge Distorted IPM Profiles with Machine Learning Algorithms", in *Proc. IPAC'18*, Vancouver, BC, Canada, Apr.–May 2018, pp. 2099–2102. doi:10.18429/JACoW-IPAC2018-WEPAK008

Content from this work may be used under the terms of the CC BY 4.0 licence (© 2024). Any distribution of this work must maintain attribution to the author(s), title of the work, publisher, and DOI.

ISBN: 978-3-95450-249-3 ISSN: 2673-5350 doi: 10.18429/JACoW-IBIC2024-FRAT1

[20] M. Sapinski, R. Singh, J.W. Storey, and D.M. Vilsmeier, "Application of Machine Learning for the IPM-Based Profile Reconstruction", in *Proc. HB'18*, Daejeon, Korea, Jun. 2018, pp. 410–415. doi:10.18429/JACoW-HB2018-THA2WE02

[21] D. Vilsmeier, M. Sapinski, and R. Singh, "Space-charge distortion of transverse profiles measured by electron-based Ionization Profile Monitors and correction methods", *Phys. Rev. Accel. Beams*, vol. 22, no. 5, p. 052801, 2019. doi:10.1103/PhysRevAccelBeams.22.052801 doi:10.48550/arXiv.1811.00371

[22] https://gitlab.com/IPMsim/Virtual-IPM

[23] https://www.3ds.com/products/simulia/cst-studio-suite

© Content from this work may be used under the terms of the CC BY 4.0 licence (© 2024). Any distribution of this work must maintain attribution to the author(s), title of the work, publisher, and DOI.